NOVA SCHOOL OF SCIENCE & TECHNOLOGY

DEPARTAMENT OF MATERIALS SCIENCE

Clara Fernandes Pacheco

BSc in Micro and Nanotechnology Engineering

Design and 3D printing of bonelike materials

MASTER IN MICRO AND NANOTECHNOLOGY ENGINEERING

NOVA University Lisbon

April, 2025

NOVA SCHOOL OF SCIENCE & TECHNOLOGY

DEPARTAMENT OF MATERIALS SCIENCE

Design and 3D printing of bonelike materials

CLARA FERNANDES PACHECO

BSc in Micro and Nanotechnology Engineering

Adviser: Isabel Ferreira
Associate Professor, NOVA University Lisbon

Examination Committee:

Chair: João Paulo Borges,
Full Professor, Nova University Lisbon

Rapporteurs: Ana Catarina Bernardino Baptista,
Senior Researcher, NOVA University Lisbon

Adviser: Isabel Ferreira,
Associate Professor, NOVA University Lisbon

MASTER IN MICRO AND NANOTECHNOLOGY ENGINEERING

NOVA University Lisbon
April 2025

Design and 3D printing of bonelike materials

ACKNOWLEDGEMENTS

O alcançar desta etapa não teria sido possível sem a colaboração, ajuda, carinho e dedicação por parte de várias pessoas ao longo de todo o meu percurso. Por esta razão, não quero deixar passar esta oportunidade para agradecer a todos aqueles que, direta e indiretamente, contribuíram para a minha chegada até aqui.

Primeiro, gostava de agradecer a todos os professores que tanto me ensinaram durante a licenciatura e mestrado. Gostaria de agradecer aos meus orientadores Isabel Ferreira e Miguel Brito pela disponibilidade e apoio ao longo deste trabalho. Gostaria também de lhes agradecer a oportunidade de trabalhar neste projeto.

Aos meus pais, Jorge Pacheco e Carla Fernandes, por me fornecerem a experiência de estudar a 300km de casa. Dedico-lhes todo e qualquer sucesso, porque por baixo de tanto sol, me fizeram chegar aqui pela sombra.

À minha irmã, Joana Pacheco, que acompanhou de perto toda esta jornada e me auxiliou em diversos momentos.

Aos meus avós, por todo o carinho e ensinamentos ao longo da vida. Em especial aos meus avós, Clara Fernandes e João Fernandes, que não estando mais entre nós fisicamente permanecem para sempre no meu coração e na minha mente. Onde quer que estejam, sei que sentem orgulho pelas minhas conquistas.

″Não tenhamos pressa, mas não percamos tempo."

(José Saramago)

ABSTRACT

Maxillofacial injuries often require customized implants that mimic natural bone in terms of their mechanical properties and degradation behaviour. This study investigates the effectiveness and durability of 3D printed parts made of calcium phosphate and zirconia-based pastes. Various compositions and mixing procedures were tested on samples produced using extrusion-based 3D printing.

The mechanical properties were assessed through compression and tensile tests, the degradation behaviour was analysed evaluating the composition of samples after being pressurised in an autoclave. Raman spectroscopy provided information on the structural characteristics of the materials. The results indicate that composition and mixing time significantly influence mechanical performance and degradation rate of the samples.

The samples with the highest calcium carbonate content exhibited improved mechanical properties and higher degradation rates. Raman analysis also indicates calcium phosphate phases and yttria-stabilized tetragonal zirconia phases. These findings suggest that 3D printing can produce implants with good mechanical strength, contributing to the advancement of patient-specific maxillofacial reconstruction.

RESUMO

As lesões maxilofaciais requerem frequentemente implantes personalizados que imitem o osso natural em termos de propriedades mecânicas e comportamento de degradação. Este estudo investiga a eficácia e durabilidade de peças impressas em 3D feitas com pastas à base de fosfato de cálcio e zircónia. Foram testadas várias composições e procedimentos de mistura em amostras produzidas através de impressão 3D por extrusão.

As propriedades mecânicas foram avaliadas através de ensaios de compressão e tração, e o comportamento de degradação foi analisado avaliando a composição das amostras após serem submetidas a pressão num autoclave. A espectroscopia Raman forneceu informações sobre as características estruturais dos materiais. Os resultados indicam que a composição e o tempo de mistura influenciam significativamente o desempenho mecânico e a taxa de degradação das amostras.

As amostras com maior teor de carbonato de cálcio apresentaram melhores propriedades mecânicas e taxas de degradação mais elevadas. A análise Raman também indica a presença de fases de fosfato de cálcio e de zircónia tetragonal estabilizada com ítria. Estes resultados sugerem que a impressão 3D pode produzir implantes com boa resistência mecânica, contribuindo para o avanço da reconstrução maxilofacial personalizada.

CONTENTS

LIST OF FIGURES

LIST OF TABLES

ACRONYMS

FDA	Food and Drug Administration
CAD	Computer-aided Design
CAM	Computer-aided Manufacturing
3D	Three-dimensional
CNC	Computer Numerical Control
AM	Additive Manufacturing
SL	Stereolithography
PM	Polyjet modelling
SLS	Selective laser sintering
FDM	Fused deposition modelling
CT	Computer tomography
MRI	Magnetic resonance Imaging
STL	Standard Template Library
2D	Two-dimensional
SBF	Simulated body fluid
BMD	Body mineral density
kN	Kilonewton
mm	Millimetres

SYMBOLS

$\boldsymbol{\pi}$	The ratio of the circumference of a circle to its diameter, having a value rounded to eight decimal places of 3.14159265 (symbol: π).
$\boldsymbol{r}$	The radius of a circle.
$\boldsymbol{h}$	Height, the measurement from base to top
$\boldsymbol{l}$	Length, the measurement or extent of something from end to end
$\boldsymbol{w}$	Width, the measurement or extent of something from side to side
$\boldsymbol{V}$	Volume, the amount of space that a substance or object occupies
$\boldsymbol{d}$	Diameter, a straight line passing from side to side through the centre of a body or figure, especially a circle or sphere
$\boldsymbol{\rho}$	Density, the degree of compactness of a substance
$\boldsymbol{\mu\rho}$	Average density

1

INTRODUCTION

This thesis focuses on the design and 3D printing of bone-like materials tailored to the specific requirements of maxillofacial implants. The work involves replicating the density and composition of natural bone material while maintaining the necessary mechanical properties and low degradation rates to ensure durability and biocompatibility. These materials are designed to serve as viable implants for replacing missing bone structures.

According to the American Food and Drug Administration (FDA), medical implants are devices or tissues that can be placed inside or on the surface of a body. These can be made of skin, bone, body tissue, or metallic, plastic, ceramic and other materials. The implants can take on a permanent or non-permanent role in the body and are used depending on the purpose for which they are intended. In Table 1, it is shown some examples of implants [1].

Table 1- Different types of implants according to U.S Food and Drug Administration [1]

Implants	Description	Examples of medical devices
Prostheses	Replace missing body parts	Maxillofacial prostheses
Implants that release medication	Releases into the bloodstream the necessary doses of a particular medicine	Contraceptive implant
Implants that regulate body function	Implantable devices that actively intervene in the function of the tissue/ body	Pacemaker
Implants that monitor body function	Implantable devices that monitor a biological parameter by transmitting information to external equipment	Intraventricular catheter

This dissertation focuses on the design of ceramic materials for prostheses, making it essential to understand their characteristics, applications, and intended purposes. According to the Institute of Maxillofacial Prosthetics and Technologies in England, a prosthesis is an artificial substitute that makes up for the loss of a certain part of the human body, such as an ear, nose, eye, or as a bone or muscle substitute that arises as a way of overcoming limitations resulting from tumours, infections or fractures to correct/fill in the missing part [2].

The term prosthesis can be particularised when discussing a more specific body region. Some examples are cranial, maxillofacial, facial, hip, and knee prostheses.

The types of prostheses available on the market are increasingly diverse. This study will focus on designing materials for maxillofacial prostheses, representing affected areas in the mandible and maxilla.

In the XXI century, the necessity of using prostheses is increasing for all age groups of the world's population and dentofacial deformities are a prevalent medical condition, affecting approximately 1 billion people. Recent studies have also shown that oral diseases affect nearly 3.5 billion people [3]. Maxillofacial injuries are a serious public health and economic problem, as their treatment may be expensive for national health systems. The maxillofacial region is particularly prone to injury because of its prominent position in the body and these injuries may have a variety of causes. Those include trauma, such as falls, assaults, sports and work injuries, congenital abnormalities and surgical excision of neoplasms. Another reason that is leading to an increase in prostheses among adults and young adults is traumatic brain injuries caused by road traffic, which are considered the main cause of maxillofacial trauma all over the world [4], [5].

The impact of maxillofacial injuries on the patient's quality of life is very profound as the deformities stand for an important clinical challenge, affecting the patient's aesthetic appearance and ability to perform everyday functional tasks [5].

The field of oral and maxillofacial surgery is dedicated to diagnosing and treating conditions affecting the oral cavity, jaw and associated structures. Despite the considerable advances and benefits offered by this technique, maxillofacial reconstruction has appeared as a challenge in dentistry for several reasons, being one of the main reasons the complexity of the maxillofacial region. It has a complicated network of bones, joints, and soft tissues, and reconstruction in this area requires an extensive understanding of facial anatomy and specialised surgical techniques. Among these techniques, orthognathic surgery, a procedure targeting the mandible, maxillary bones and both upper and lower jaws, plays a crucial part [5]. In addition to the broader maxillofacial structures, the alveolar bone plays a vital role within the maxilla and mandible, providing foundational support for the teeth and directly influencing both function and aesthetics in maxillofacial reconstruction, in Figure 2 it is possible to see a diagram of the tooth cut vertically. This bone is formed in association with the development and eruption of dental elements and can be gradually resorbed when teeth are lost, as seen in Figure 1. It can therefore be said that the alveolar process is a tooth-dependent structure. In general, alveolar bone is composed of two-thirds inorganic substances (mostly calcium and phosphate minerals) and one-third organic matrix (19% type1 collagen). Despite its constant renewal, its organisation and shape are practically

maintained from infancy to adulthood and despite its support, this bone is the least rigid from the human face [6].

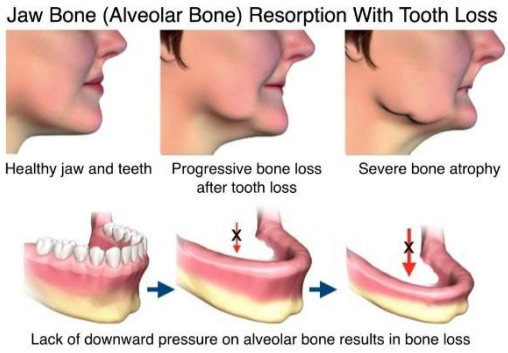

Figure 1-Resorption of the Jawbone with tooth loss [25]

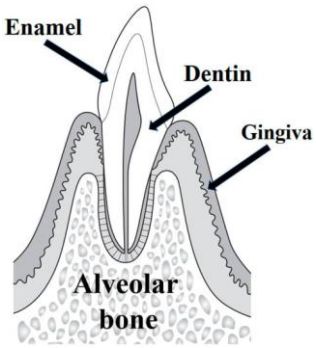

Figure 2- Diagram of a tooth cut vertically [26]

This surgery can reconstruct and restore structural integrity, allowing patients to regain masticatory, respiratory and phonetic function, playing a key role in aesthetic and psychological rehabilitation. Furthermore, the successful reconstruction of bone defects in the maxillofacial region can prevent long-term complications such as facial deformities, temporomandibular joint problems, and challenges in placing dental implants, all contribute to patients' general health and well-being. As a result, this intervention plays a critical role in restoring form, function, and overall quality of life, making it one of the most essential techniques in maxillofacial surgery [5].

In today's era and given the unique structural properties and challenges associated with the alveolar bone, there has been a rapid trend towards digitalisation in dentistry, as in many other industries. In this way, adopting digital tools in this area has become particularly valuable. Technologies such as computer-aided design and manufacturing (CAD/CAM), digital data acquisition, and three-dimensional (3D) printing have greatly improved the practical principles of dental implants [7].

Two different technologies have been used to carry out industrial and medical production. Subtractive manufacturing or computer numerical control (CNC) milling and additive manufacturing (AM/3D printing). Despite the success of subtractive manufacturing in dental implantology, this technology is very costly due to the wasted raw materials in the process and the cutting tools wear, making them suitable for only a limited number of milling cycles. It is also not possible to produce complex geometrical and hollow structures with this technology. The processes in CNC milling involve cutting through refabricated discs or blocks until reaching the desired form, while 3D printing constructs objects via sequential material layering, following a digital 3D model and turning it into a 3D physical object. This technology is a better option for creating complex and hollow structures as well as being more economical, efficient and environmentally friendly [7].

This technology offers new possibilities in the treatment of complex structures, such as the alveolar bone, through anatomical models and personalised guides adapted to the needs of each patient. There are different AM technologies, each having its advantages, challenges, material types, and printing procedures, although their basis is layer-by-layer production. Normally, this technology is

categorised into solid, liquid and powder-based approaches based entirely on input materials [8]. Some examples of AM technologies are:

- Liquid-based 3D printing technology
    - Stereolithography (SL): the most used 3D technique. A layer of liquid photopolymer or epoxy resin in a model-building platform is cured by a low-power ultraviolet (UV) laser.
    - Polyjet modelling (PM): jetting liquid photo-polymer materials in ultra-thin layers (16 µm) onto a build tray layer by layer, until the model is completed.
- Powder-based 3D printing technology
    - Selective laser sintering (SLS): used to create metal, plastic, and ceramic models, by multiple steps, which require long fabrication time and high cost.
    - 3D printing (binderjet): uses a print head to disperse a binder onto powder layers selectively.
- Solid-based 3D printing technology
    - Fused deposition modelling (FDM): Similar to SL, the main difference is that the layers are deposited as a thermoplastic extruded from a fine nozzle by computer control [8].

These AM techniques offer various materials with differing precision levels suited to the biomedical industry. The standard procedure for 3D printing biomedical products begins with:

1. Creating a 3D model, using patient-specific medical images from sources like computer tomography (CT) or magnetic resonance imaging (MRI) scans.
2. These images are transformed into a virtual model through CAD software, resulting in a digital file typically saved in standard template library (STL) format.
3. The STL file is then sliced into 2D cross-sectional layers, each representing a portion of the 3D model.

An AM machine uses this sliced data to build the 3D object layer by layer, accurately placing materials, biomolecules, or even living cells to recreate the design. These items might need post-processing to enhance their structural qualities or eliminate support materials in certain situations [9].

In dentistry, over the past 20 years, AM has been used to link diagnostic evaluation, treatment, planning and manufacturing phases, significantly improving the overall treatment strategy, postsurgical care and clinical survival. Furthermore, the digital workflow has shown significant workload reduction in dental practitioners and enhanced patient satisfaction with dental care in the modern era [7]. In maxillary surgery, AM plays a pivotal role in two major areas: reconstruction (where it restores the normal anatomy of the maxillofacial region) and orthognathic surgery (where 3D-printed surgical guides aid in treating skeletal malocclusion). In implantology, AM technologies have revolutionised practices such as dental implantation (customised dental implants), auto-transplantation, and allogenic tooth transplantation. These advances also include specially designed implant drill, enabling precise and patient-specific treatment solutions [10].

However, while AM presents significant benefits, there are specific disadvantages when it comes to its application in dentistry. For instance, MRI equipment cannot gather the necessary data for AM therapies in patients with metallic implants, limiting the creation of patient-specific models. Another drawback is that some materials are incompatible and cannot be processed by AM. Manufacturing these materials for replacement and fabrication may not be simple or economical. Certain studies state that

there are aesthetic problems with the mandibular AM dentures' shape. Making sure the product surface is of adequate quality and satisfying post-processing standards are the two most important areas that need improvement. The structures' accuracy varies depending on the materials utilised, the production technique, and the geometries being copied. Ongoing research is focused on alternative methods of current fabrication techniques that could enable the creation of nanoscale structures. Another challenge is the adhesion of printed denture teeth, as bond strength is crucial. According to reports, the bond strength achieved by traditional processing is higher than that of printed teeth bonded to a printed denture base. Another difficulty is the standardisation issue for AM-fabricated surgical models utilised in actual clinical procedures. International standardisation of AM models in terms of size, materials, machine types, and disease types also provides better communication among the operators in different hospitals and countries. However, following surgery, immunological rejection or inflammation may still be evident, necessitating a second surgery for the patient [10].

Biomimetics, which imitates elements, models, strategies and systems from nature by solving simple to complex human problems is a significant inspiration for these innovations. Nature keeps immeasurable innovation and inspiration, which are categorised as visual (shapes and structures) and functional (functionality or muti-functionality) inspirations [11]. It has in view to restore the structure and function of damaged teeth using materials that closely mimic natural teeth. One of the biggest benefits of biomimetics is reducing the number of invasive techniques that keep the natural tooth structure as much as possible by using materials that closely resemble the structure and characteristics of teeth. Materials like composite resins, ceramics and dental adhesives, have been developed to mimic the natural properties of teeth, such as their strength, elasticity and durability [12].

For a particular implant application, the selection of material will generally be a compromise to meet many different properties that are required. However, the way the tissue at the implant site reacts to the biochemical disruption caused by a foreign material is always the most crucial factor. In additive manufacturing, the selection of materials is crucial to meet the specific requirements of each application. In applications for implants, metals and ceramics are preferred and should be inert [13]. According to Schmidt et al. (2001) [13] an ideal bone implant material should have a biocompatible chemical composition, excellent corrosion resistance, acceptable strength, high resistance to wear, and high modulus of elasticity. Dental implants are made of a range of materials. Nonetheless, titanium is typically used to make them because it promotes a strong and useful bond between the implant's surface and the bone [14]. Polymers are used when a material is required to be biodegradable to provide tissue growth. When one material by itself cannot offer function, composite implants made of a combination of materials may be required. In calcium phosphate the calcium and phosphate compounds give it a close resemblance to the materials found in human bone. This similarity eases a direct chemical bond with the bones. But compared to human bone, calcium phosphate has a higher compressive strength [10], [14]

The AM of ceramics gained more interest as it hits the potential to be developed into biomedical products, mainly implants and scaffolds, which can be made similar to or mimic the replaced body tissue. This is accomplished by choosing materials that have the same chemical and physical characteristics to promote osteoconduction (the ability to allow the deposition of mineralised tissue on the

surface) and osseointegration (direct bond between the implant surface and bone tissue, without a fibrous layer in between), and by creating a scaffold structure that resembles bone to induce osteointegration, processing, and appropriate structural alteration to promote quicker healing [11], [14]. Some features of these materials make them very attractive to use in dentistry. These are similar to natural dentition properties, such as compressive strength, thermal conductivity, radiopacity, colour stability, and aesthetics. However, these materials are brittle, hard and sometimes difficult to process [15].

One ceramic material that is used and has received a lot of research attention is calcium phosphate. This biomedical material is attractive due to its chemical similarity to bones and teeth, its good biocompatibility, and its chemical components' nontoxicity. Calcium phosphates belong to the group of bioactive synthetic materials and their most frequently used are the hydroxyapatite and the tricalcium phosphate. They are commonly used due to their osteoconductivity, crystallographic structures and chemical composition similar to the osseous tissue. They are classified according to their resorbable quality, the extent of degradation in vivo. Hydroxyapatite has been described as “non-resorbable” and tricalcium phosphate has been described as “resorbable.” This material also shows a positive interaction with living tissue that includes the differentiation of immature cells towards bone cells. These materials also have chemical bonding to the bone along the interface, thought to be triggered by the adsorption of bone growth-mediating proteins at the biomaterial surface. Some of the applications of calcium phosphate are the repair of periodontal defects, augmentation of alveolar bone, sinus lifts, tooth replacement, and repair of large bone defects caused by tumours. In tissue engineering, it is also used as a scaffold for bone or dentin regeneration [15].

Although AM has been successfully applied in many medical fields, there are still issues that need to be addressed including enhanced biocompatibility, functionality, long-term limb replacement and improving performance through technological innovation. Consequently, studies are conducted to reduce production time and to provide improved software for more precise outcomes. Future expectations suggest that dental research will particularly focus on AM technology development to accelerate the increase in the number of novel dental materials, tools, implants, and next generation modelling strategies [9], [10].

In conclusion, 3D printing has revolutionised the field of maxillofacial mimetics by significantly improving the precision, functionality, and aesthetics of facial reconstruction and prosthetics. Its capability to create highly personalised and anatomically precise models enhances patient outcomes, leading to better physical appearance, restored functionality, and improved quality of life. This technology aids pre-surgical planning speeds up treatment timelines, and reduces errors, benefiting both surgeons and patients. Despite these advancements, challenges such as material compatibility, manufacturing limitations, and standardisation persist, necessitating continued innovation and research. The continued research and development in 3D printing technologies are pivotal to addressing existing challenges and expanding the scope of its application in maxillofacial mimetics. This way, 3D printing is not merely a technological advancement but a paradigm shift in maxillofacial surgery and prosthetics.

2

MATERIALS AND METHODS

This research will focus on the design of 3D printing materials that mimic natural bone in density, mechanical and degradation properties to ensure the effectiveness and durability of implants. The goal is to answer the question, 'Are 3D-printed implants effective in functionality and durability for patients with maxillofacial injuries?' Inspired by the quest to develop materials that imitate maxillofacial parts according to implant needs. To study the materials, the following shapes were printed on the 3D printer:

These pieces were prepared by making a 6-gram paste where 65% was a zirconia-based paste (whose composition was developed for other projects and not disclosed) and a series of varying proportions of diverse materials were combined with the starting material, including Calcium Phosphate, Calcium Carbonate type I and Calcium Carbonate type II, Graphite. The mixtures were mixed either manually or mechanically and with different mixing times, allowing to study the effects of mixing method and duration on the final properties of the mixture. Subsequently, the paste was transferred into a syringe and using a needle (with different diameters, 0.51mm, 0.84mm, 1.65mm), and a hollow cylindrical structure, 9 mm height and 9 mm external diameter was printed (Focus 3D Food Printer, byFlow, Netherlands), using the default printing parameters and different printing modes (+360-360, where the syringe changes direction at the end of each line and +360 where the syringe always follows the same direction). The printed pieces were left to air dry and were then sintered in an oven (Nabertherm LHT 08/18). The sintering was processed at 1250ºC. The heating up ramp was defined as a gradual rising during 7 hours to the defined temperature, remaining at this temperature for 2 hours, after which it gradually cooled down to 0 °C.

Five of these pieces were produced for each composition studied:

1. **Influence of the mixing procedure**
    a. paste with 35%wt calcium phosphate
        i. paste mixed manually for 5 minutes
        ii. paste mixed with a mixer for 5 minutes
        iii. paste mixed with a mixer for 15 minutes
    b. paste with 25% wt calcium phosphate
        i. paste mixed with a mixer for 5 minutes
        ii. paste mixed with a mixer for 15 minutes

2. Influence of the paste composition

a. 25% wt calcium carbonate I, mixed for 5 minutes with a mixer
b. 25% wt calcium carbonate II, mixed for 5 minutes with a mixer
c. 35% wt calcium carbonate I, mixed for 5 minutes manually
d. 35% wt calcium carbonate II, mixed for 5 minutes with a mixer
e. 20% wt graphite and 30% wt calcium carbonate I, mixed for 5 minutes manually
f. 35% wt calcium phosphate, mixed for 5 minutes manually
g. 35% wt calcium phosphate, mixed for 5 minutes manually, with 50% infill
h. 35% wt calcium carbonate, mixed for 5 minutes manually, with 50% infill

3. Influence of infill

a. 35% wt calcium phosphate with 100% infill
b. 35% wt calcium phosphate with 50% infill
c. 35% wt calcium carbonate type I with 100% infill
d. 35% wt calcium carbonate type I with 50% infill

4. Density of the produced pieces

After each piece was produced and had waited to dry, the outer diameter, inner diameter, and height measurements were taken with the help of a digital calliper. A scale was used to measure the weight. The volume, density, average density, and standard deviation were calculated based on these values. The volume was obtained with the following formula for the hollow pieces:

$$V = \frac{\pi({d_{outer}}^2 - {d_{inner}}^2) * h}{4} \; x \; 10^{-3} \; (\mathrm{cm}^3) \; (1)$$

$d_{outer} \; - \; outer \; diameter \; (mm); \; d_{inner} \; - \; inner \; diameter \; (mm); h - height \; (mm)$

The density and average density were obtained, respectively, using:

$$\rho = \frac{m}{V} \; (2) \qquad\qquad \mu\rho = \frac{\rho}{x} \; (3)$$

$\rho - \; density \; (g/\mathrm{cm}\ 3); \; \mu\rho - \; average \; density; \; x - \; number \; of \; analysed \; samples$

To define the volume shrinkage, these measurements were taken before and after the sintering.

5. Mechanical tests

For the compression tests, five pieces from each group were analysed, submitting them to a continuous (0.5mm/min) compression force until it broke. Each piece was put between two plates and an external uniaxial compression force was applied to the material. During this, information such as the applied load and the resulting deformation was recorded, allowing the construction of the stress-strain diagram.

To the traction tests an increasing uniaxial load was applied in a specific specimen until it fractures. The length is recorded as a function of the load applied to and after data processing it is possible to obtain a stress versus strain curve.

For the compression tests, the parameters used were

- Loading speed: the rate at which the compressive force was applied to the specimen, set to 0.5 mm/min;

- Maximum load: the predefined limit to avoid overloading the sample, set at 0.01kN for the y-axis and 0.01mm for the x-axis;
- Sample dimensions: the geometry and size of samples((9x9)mm, hollow and full);
- Sampling interval: the distance between points at which measurements are taken, set at 50 msec;
- Data acquisition rate: the frequency at which data points were recorded, 20Hz

These parameters were carefully chosen to ensure the accuracy and reproducibility of the results.
For the full pieces the volume was measured using:

$$V = \pi * r^2 * h \ (4)$$

$h - \ height$

and traction pieces volume were measured using:

$$V = l * w * h \ (5)$$

$l - lenght; w - width; h - height$

6. Degradation tests

Regarding degradation tests, 5 printed pieces with 35%wt calcium phosphate mixed for 5 minutes manually were put in an autoclave with 30 mL of SBF (simulated body fluid). The autoclave was then placed in an oven for 5 hours at 134ºC (the equivalent of 15/20 years in the organism). The same process was repeated for paste with 35%wt calcium carbonate mixed for 5 minutes manually.

7. Chemical analysis

Raman spectroscopy was also used to analyse these materials. This technique is a non-destructive chemical analysis and provides detailed information about chemical structure, phase, polymorphy, crystallinity and molecular interactions. It is based on the interaction of electromagnetic radiation with the material, where a monochromatic radiation font (laser) of a certain frequency scatters when it hits the material. The chemical and structural information obtained from this high-resolution technique allows the identification of different components.

3

RESULTS AND DISCUSSION

3.1 Printed pieces

Before printing the pieces, a design step was performed in the software Simplify3D and then a GCode file was generated. Figure 4 illustrates the design of the 50% infill design in the software.

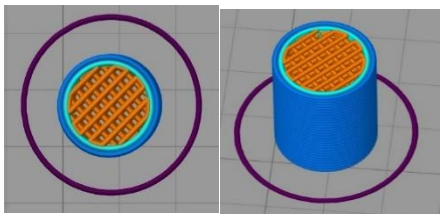

Figure 3- Example of 50% infill design

Figure 4 represent a sample of 35% wt calcium phosphate and 50% infill before a) and after sintering b) and c).

a) b) c)

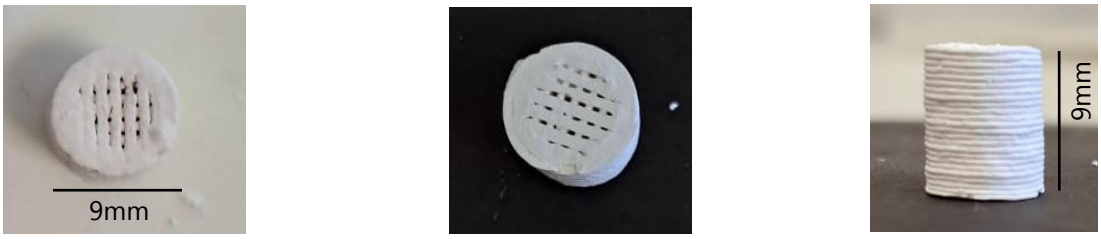

Figure 4- 35% wt calcium phosphate with 50% in fill before sintering; and after sintering, a) top view before sintering, b) top view after sintering and c) side view after sintering

3.2 Mechanical Tests

3.2.1 Compression Tests

Through the mechanical tests, it was possible to obtain data to create a stress-strain curve. This data was the time, in seconds, the Force, kilonewton, kN, and Stroke, millimetres, mm. By dividing the Force data with the area of the sample, it was possible to obtain the Stress values. To acquire the Strain values, the values 'stroke' was divided by the samples' height, as mentioned in Materials and Methods

The diagram of Figure 5 shows how the material deforms in response to the applied stress and provides information about the material's mechanical properties such as elastic modulus, yield strength and compressive strength. It can be obtained from both compression and traction tests. [16]

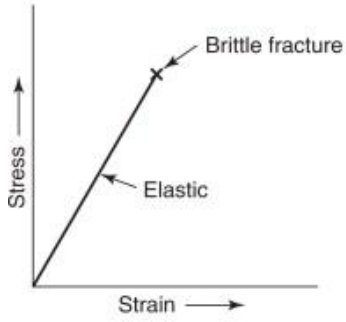

Figure 5- Stress vs Strain curve for ceramics [17]

The Young modulus is a mechanical property that measures the stiffness of a solid material, and it defines the ratio between stress and strain. Through Figure , it is possible to see that the Young modulus was obtained by performing a linear regression on the elastic region of the stress vs strain graphic. This region corresponds to the portion of the data where the relationship between stress and strain is approximately linear, allowing the slope of the fitted line to be interpreted as Young's modulus. The maximum stress was identified as the highest point on the stress vs strain curve before the fracture. It represents the peak stress the material can take during the test.

The Young modulus is calculated as

$$E = \frac{\sigma}{\varepsilon} \quad (6)$$

σ being the Stress and ε the Strain.

The maximum Force is equivalent to the maximum stress. The fracture point marks the end of the stress-strain curve and represents the stress at which the material fails. In Figure 6, it is possible to see that the curve drops sharply after the maximum point, which indicates a sudden fracture typical of ceramic materials.

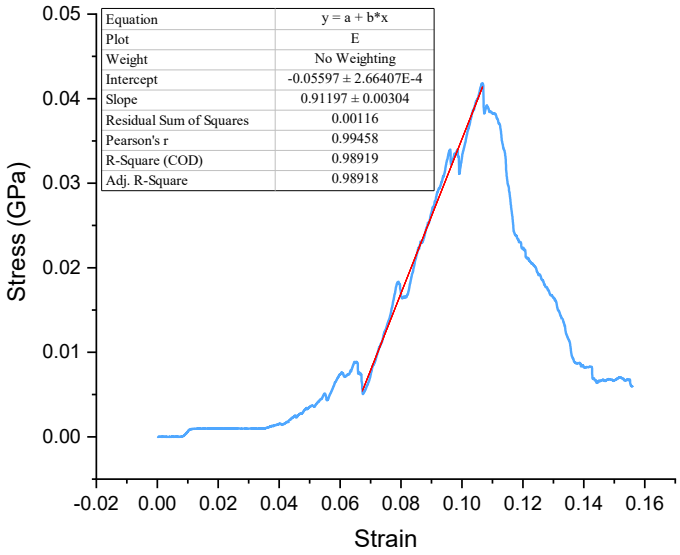

Figure 6- Example of stress vs strength curve obtained for the pieces produced.

The mechanical properties of the specimens obtained under different preparation conditions were analysed and summarised in the following Tables.

3.2.1.1 Influence of the paste's composition

The main different compositions analysed contain a base paste with – 1) calcium phosphate; - 2) calcium carbonate; - 3) calcium carbonate and graphite. The results are shown in the following tables were:

- Young Modulus (MPa): represents the stiffness of the material measured in megapascal; the value is the average value of the samples measured;
- Critical value (MPa): indicates the stress level at which the materials fail; the value is the average value of the samples measured;
- +360 -360: indicates that the printing mode was done by changing direction at the end of each line;

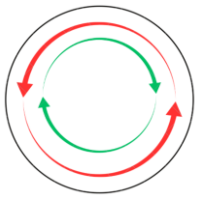

Figure 7- Printing mode changing the direction (+360-360).

- +360: indicates that the printing mode was done by not changing the direction of each circle, that is, the printing was continuous;

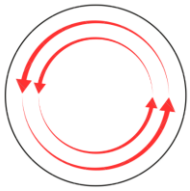

Figure 8- Continuous printing mode (+360)

- Autoclave: means the material was treated in an autoclave;
- Needle: denotes the diameter of the needle of the syringe used.

The rows outline the preparation methods and their respective durations:

- 5 minutes by hand: provides results for materials mixed manually for 5 minutes;
- 5 minutes with a mixer: prepared with mechanical mixing for the same duration;
- 15 minutes with a mixer: includes data for mechanically mixed materials for 15 minutes.

Table 2 shows the average results obtained for the pieces with 35%wt and 25% wt calcium phosphate.

Table 2- Mechanical properties of the pieces with 35% wt and 25% wt calcium phosphate.

Paste mixture	Young Modulus (MPa)	Critical Value (MPa)	+360 -360	+360	Auto-clave	Needle diameter (mm)	
						0.84	1.65
35% wt calcium phosphate							
5 min by hand	1333 ± 411	22 ± 6	✓			✓	
	1056 ± 376	35 ± 8		✓		✓	
	154 ± 36	7 ± 1	✓		✓	✓	
	686 ± 125	42 ± 11	✓				✓
5 min with mixer	1102 ± 169	25 ± 2	✓			✓	
15 min with mixer	1819 ± 906	18 ± 5	✓			✓	
25% wt calcium phosphate							
5 min with mixer	687 ± 189	14 ± 5	✓			✓	
15 min with mixer	624 ± 98	16 ± 8	✓			✓	

For 35%wt calcium phosphate, it is possible to see that the group for '5 min by hand' that went to the autoclave has the lowest Young modulus average, (154 ± 36) MPa. In contrast, the group with the highest average Young modulus is the 35%wt calcium phosphate mixed with a mixer for 15 minutes, (1819 ± 906) MPa. The reason could be due to a better mixing of pastes, leading to more homogeneously distributed components, which enhances the uniformity of the mixture. The average Young modulus is higher for the group '15min with mixer' and so is the critical value.

Comparing results for 25%wt with the ones attained for the 35% calcium phosphate samples, it is possible to observe that, overall, the group with the highest Young modulus is the 35% wt calcium phosphate '15 min by mixer'.

Table 3 compares the mechanical properties of the group pieces with 35% wt and 25% wt of calcium carbonate type I, with those produced with 35% wt of calcium carbonate type II, and 30 wt calcium carbonate type I with 20% wt of graphite.

Table 3- Mechanical properties of the pieces with percentages of calcium carbonate type I and type II and graphite

Paste mixture	Young Modulus (MPa)	Critical Value (MPa)	+360 -360	+360	Auto-clave	needle diameter (mm)	
						0.84	1.65
35% wt calcium carbonate type I							
5 min by hand	1972 ± 455	29 ± 4	✓			✓	
	1580 ± 347	40 ± 3		✓		✓	
	123 ± 14	4 ± 0.5	✓		✓	✓	
	791 ± 146	25 ± 3		✓			✓
25% wt calcium carbonate type I							
5 min by hand	2242 ± 345	26 ± 12	✓			✓	
35% wt calcium carbonate type II							
5 min with mixer	2548 ± 961	29 ± 3	✓			✓	
30% wt calcium carbonate type I and 20% wt graphite							
5 min by hand	162 ± 48	7 ± 1	✓			✓	

For 35% wt calcium phosphate, it was not possible to do samples for 5 minutes with a mixer and 15 minutes with a mixer as the paste and the calcium carbonate did not mix at all.

From the data presented in Table 3, we can observe that the group with the highest average Young's modulus has a value of (2548 ± 961) MPa. In contrast, the group with the lowest average Young's modulus presents a value of (123 ± 14) MPa. The pieces subjected to the autoclave exhibit the lowest Young's modulus values, (123 ± 14) MPa and (154 ± 36) MPa, for 35% calcium carbonate and 35% calcium phosphate, respectively. Notably, the modulus is slightly higher for the pieces containing calcium carbonate. The discrepancy in the values of these groups from the others can be explained by the degradation the pieces suffered in the autoclave.

The average Young modulus for 25% wt calcium carbonate type I is (2242 ± 345) MPa, which is higher compared to the group of 35% calcium carbonate type I '5min by hand' with the same printing

mode. For the value obtained for 25% calcium carbonate type II, (2548 ± 961) MPa, it is possible to observe that this value is higher than the ones obtained for all the samples of calcium carbonate type I. Comparing the value obtained for 20% wt graphite and 30% wt calcium carbonate with all the other values, it is possible to observe that, besides the samples that went to the autoclave, this value is the lowest.

The results also highlight the influence of the printing process, including different movement patterns of the syringe and needle size. Three main printing modes were evaluated: continuous printing, where the syringe moves in a single direction (+360º); a forward and backwards process, where the syringe rotates +360º and then –360º; and variations in needle size.

When comparing needle sizes for the same continuous printing mode (+360º), it appears that smaller needle diameters lead to improved mechanical properties. Conversely, when using a bidirectional printing process (+360º, –360º) with the same needle size, samples exhibited a higher Young's modulus but lower ultimate strength. This might be due to better bonding between printed lines and was consistently observed in both calcium phosphate and calcium carbonate samples.

However, this consistency did not extend to samples with varying percentages of calcium phosphate and calcium carbonate (types I and II). For instance, reducing the calcium carbonate type I content from 35% to 25% led to an increase in compressive strength. This trend was not observed in samples containing calcium phosphate, where a reduction in added material was expected to decrease mechanical strength. This unexpected behaviour may be due to inconsistencies in mixing or other unidentified factors.

Interestingly, calcium carbonate type II samples demonstrated higher compressive strength, possibly due to the smaller particle size compared to type I.

Besides the influence of composition also the design of the pieces may also influence the mechanical resistance. This was studied by varying the infill of pieces.

3.2.1.2 Influence of infill

The influence of infill in the mechanical properties is shown in Table 4. There is 100% and 50% infill, while the preparation method is the same, mixed 5 minutes by hand with +360, -360 printing.

Table 4- Mechanical properties of samples with 35% calcium phosphate and 35% calcium carbonate for different infill.

Infill	Young Modulus (MPa)	Critical Value (MPa)	+360	Needle diameter (mm)
				0.84
35% wt calcium phosphate				
100%	26 ± 7	2 ± 1	✓	✓
50%	15 ± 6	0.6 ± 0.1	✓	✓

35% wt calcium carbonate				
100%	3 ± 0.7	0.3 ± 0.04	✓	✓
50%	5 ± 1	0.4 ± 0.05	✓	✓

Comparing the samples of 35% wt calcium phosphate with 100% and 50% infill design, the Young modulus is slightly higher for the full design. Comparing these values with the values obtained for 35%wt calcium phosphate but with a hollow cylinder design, (1056 ± 376) MPa, these are much lower.

For the samples of 35% wt calcium carbonate, the difference between the values of the Young modulus of the two designs is lower. In this case, the one with the higher Young modulus is the 35% wt calcium carbonate with 50% infill. These values are also much lower than the 35%wt calcium carbonate with a hollow cylinder design, which is (1580 ± 347) MPa.

Table 5 illustrates the Young's modulus and compressive strength for the mandible bone.

Table 5- Range of Young modulus and compressive strength for mandibular bone [18]

	Young's Modulus (MPa)	Compressive strength (MPa)
Trabecular bone	10- 500	4- 12
Cortical bone	3000-30000	130- 125

The values obtained that come closest to those of trabecular bone are both the samples from calcium phosphate and calcium carbonate that underwent autoclaving. The average Young modulus for these samples is (154 ± 36) MPa and (123 ± 14) MPa, respectively. Another sample in the range for the Young modulus of trabecular bone is 20% graphite and 30% calcium carbonate with an average Young modulus of (162 ± 48) MPa. When it comes to the compressive strength, these samples also fit in the range showed in the table, (7 ± 1) MPa, for 35% calcium phosphate and 20% graphite and 30% calcium carbonate and (4 ± 0.5) MPa, for 35% calcium carbonate.

For the cortical bone, none of the values obtained are within the range of values presented, but the one that comes closer is the sample of 35% wt calcium carbonate type II with an average Young modulus of (2548 ± 961) MPa. For the compressive strength, the value for this sample is much lower than the range on the table, (29 ± 3) MPa.

3.2.2 Density

The density of the samples was also measured so that it could be compared with the density of the jawbone.

Table 6 shows the values of average density values obtained for all the samples.

Table 6- Density of different composition samples.

Paste mixture	Density (g/cm^3)	+360 -360	+360	Needle diameter (mm)		
				0.51	0.84	1.65
35% wt calcium phosphate						
5 min by hand	2.5 ± 0.2	✓			✓	
	2.6 ± 0.2		✓		✓	
	2.4 ± 0.3		✓	✓		
5 min with mixer	2.5 ± 0.1	✓			✓	
15 min with mixer	2.6 ± 0.3	✓			✓	
35% wt calcium carbonate type I						
5 min by hand	2.1 ± 0.2	✓			✓	
	1.9 ± 0.04		✓		✓	
	2.0 ± 0.2	✓				✓
25% wt calcium phosphate						
5 min with mixer	2.7± 0.2	✓			✓	
15 min with mixer	2.7± 0.08	✓			✓	
25% wt calcium carbonate type I						
5 min by hand	2.7 ± 0.1	✓			✓	
25% wt calcium carbonate type II						
5 min with mixer	2.6 ± 0.1	✓			✓	
20% wt graphite and 30% wt calcium carbonate type I						
5 min by hand	1.3 ± 0.1	✓			✓	

Comparing all the density values, we see that they are all close, with the range of values being [1.3 ± 0.1; 2.7 ± 0.2] g/cm^3.

Comparing all values acquired with the jawbone density values, seen in Table 16, it is possible to observe that the value for average density of 20% graphite and 30% calcium carbonate type I, (1.3 ± 0.1) g/cm^3, is the closest to the mandibular body BMD, (1.386 ± 0.320) g/cm^3. The average density value for 35% calcium carbonate type I with +360 design with a needle with 0.84mm diameter, (1.9 ± 0.04) g/cm^3, is the closest to the anterior mandible BMD, (1.470 ± 0.271) g/cm^3.

Table 7- Bone mineral density (BMD) of different mandible regions [19]

Bone	BMD (g/cm^3)
Anterior mandible	1.470 ± 0.271
Mandibular body	1.386 ± 0.320
Mandibular ramus	0.835 ± 0.223

3.2.3 Tensile tests

In this study, traction tests were also run through, but they failed. Through Figure 9, it is possible to see a sample of a) 35% calcium phosphate, b) 35% calcium carbonate type I and c) 35% calcium carbonate after the test.

Figure 9- Samples for traction tests of a) 35% calcium phosphate; b) 35% calcium carbonate type1; c) 35% calcium carbonate after the test

In Figure 9c), it is possible to observe that the sample broke at the 90-degree vertex. The failure occurred due to stress concentration, as such geometrical features tend to accumulate stress under tensile loading. The tensile tests were unsuccessful due to the incorrect design of the samples and due to lack of time was impossible to produce new samples for repeating the measurements.

3.3 Raman Spectroscopy

The Raman analysis allows to identify the composition of non-metallic samples. Since it's a punctual analysis, uniformity of composition can be ascertained by measuring different points of the samples. In the present study, the curves of different colours in the spectrum represent analyses performed at various points on the sample. The overlap of peaks between different points of the sample suggests that all contain a combination of these phases, but with possible variations in the proportion of each depending on the location analysed. In every figure, it is possible to see a spectrum of the analysed sample and a greyed-out region that corresponds to the area where the analysis was performed. To verify the different components of the spectra, the peaks were identified ([20], [21], [22], [23], [24]).

The Raman spectrum for 35% wt calcium is shown in Figure 10. The corresponding peaks to the monoclinic phase, identified as m-ZrO_2, are 340 cm^{-1} and 600 cm^{-1}. The tetragonal phase, t-ZrO_2, peaks are present at 149 cm^{-1}, 292 cm^{-1} and 390 cm^{-1}. The peak associated with the cubic phase, c-ZrO_2, 634 cm^{-1}. The peak at 217 cm^{-1} corresponds to the vibrational mode v2 Zr-O, while 500 cm^{-1} is due to

v1 Zr-O. The peak at 750 cm^{-1} is due to v4 C-O (HA), 968 cm^{-1} represents v1 P-O (β -TCP) and 1093 cm^{-1} is due to v3 P-O (HA).

The results show a good uniformity of the composition for all measurements taken, independently of the pastes mixture, by hand, with mixer for 5 minutes or 15 minutes, and for the different positions inside the samples, revealing a homogeneous structure.

Interestingly, the main composition shown for samples with 35% wt of calcium phosphate is the base paste zirconia, which main phase is the tetragonal with a small peak of monoclinic phase. The calcium phosphide appears as β -TCP and a hydroxyapatite ascribed to the peaks of 968 cm^{-1} and 1093, respectively.

35% wt calcium phosphate

mixed by hand for 5 minutes

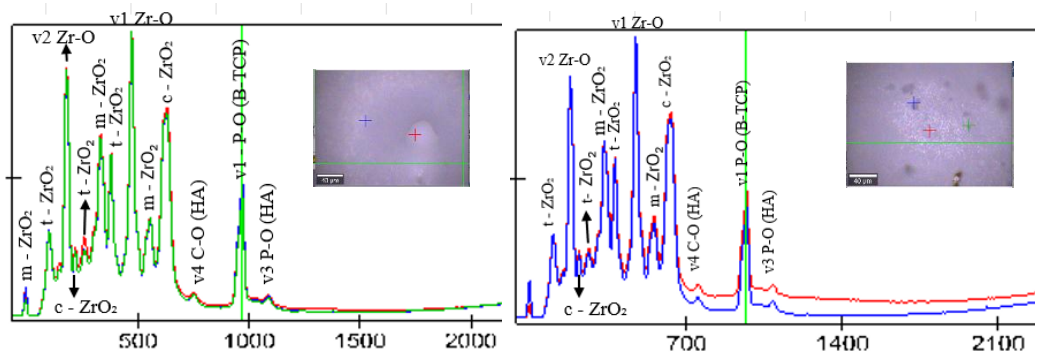

Raman shift (cm^{-1})

mixed for 5 minutes with a mixer.

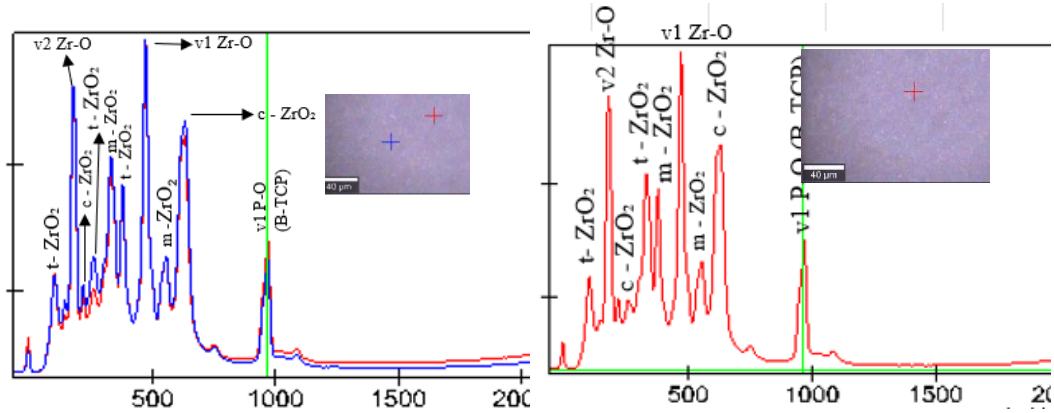

Raman shift (cm^{-1})

mixed for 15 minutes with a mixer

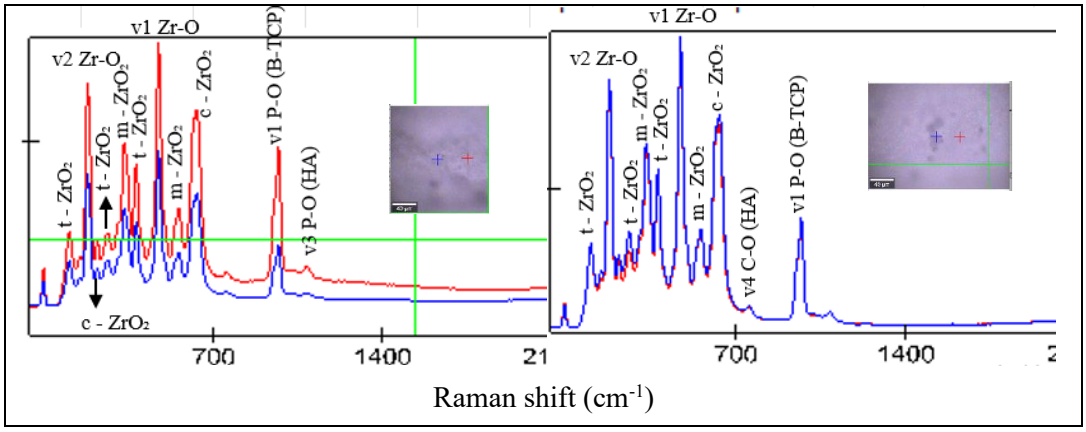

Figure 10- Comparison of the Raman spectra as a function of paste mixture and for 35% wt calcium phosphate composition.

The following figure, Figure 11, represents the spectra for 25% calcium phosphate mixed with a mixer for 15 minutes. It is possible to see that the peaks associated with Zirconia are 170 cm^{-1}, 340 cm^{-1} and 612 cm^{-1} for m-ZrO_2, 634 cm^{-1} for c-ZrO_2 and 149 cm^{-1}, 292 cm^{-1} and 390 cm^{-1} are associated with t-ZrO_2. It is also possible to observe a v2 Zr-O peak at 217 cm^{-1} and v1 Zr-O at 500 cm^{-1}. There´s also a β-tricalcium phosphate group, v1 P-O (β-TCP), at 968 cm^{-1}. The peaks at 1050 cm^{-1} and 1080 cm^{-1} represent v3 P-O (HA) and v1 C-O, respectively.

These samples also demonstrate a good uniformity of composition across all measurements taken.

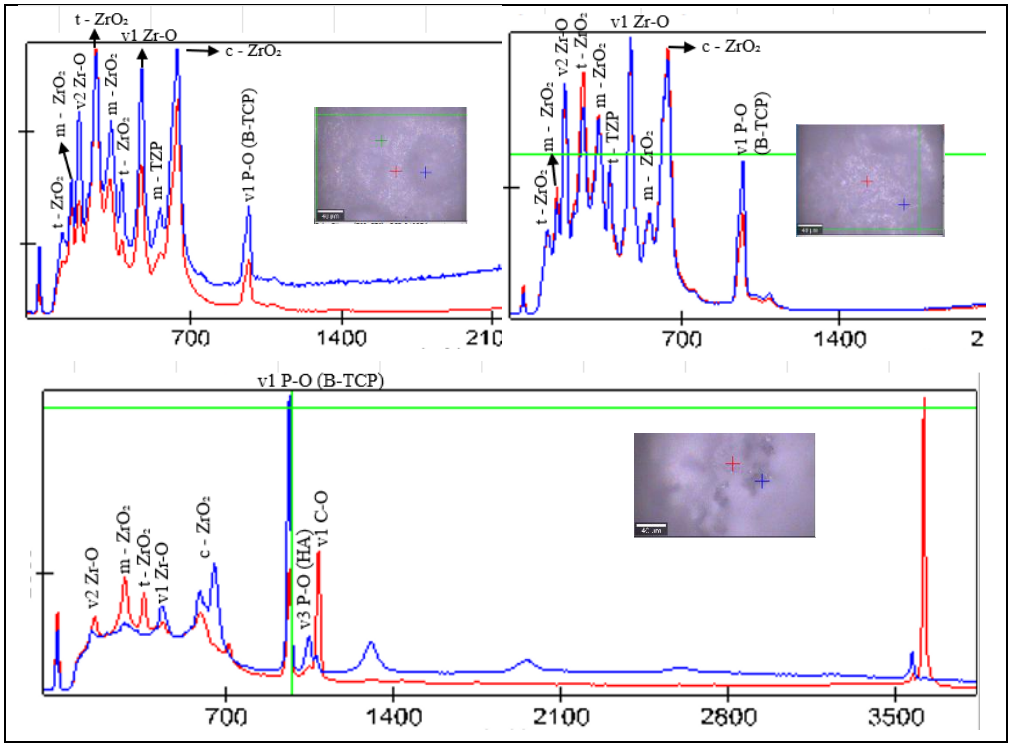

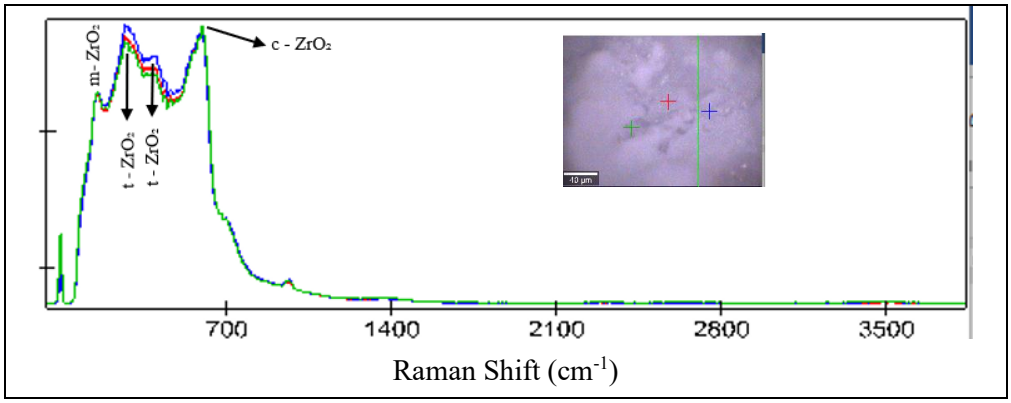

Figure 11- Raman spectra for 25% calcium phosphate mixed for 15 minutes with a mixer for different spots of the sample.

The following spectra represent the Raman analysis for the calcium carbonate samples. Figure 12 represents the spectrum for 25% calcium carbonate type II mixed for 5 minutes with a mixer and the peaks at 180 cm^{-1}, 325 cm^{-1}, 380 cm^{-1}, 550 cm^{-1} and 600 cm^{-1} represent m-ZrO_2 component. The t-ZrO_2 peaks are at 260 cm^{-1}, 410 cm^{-1} and 650 cm^{-1}. It also has a peak at 968 cm^{-1} due to vibrational mode v1 P-O (β -TCP) and at 1090 cm^{-1} associated with v3 P-O (HA).

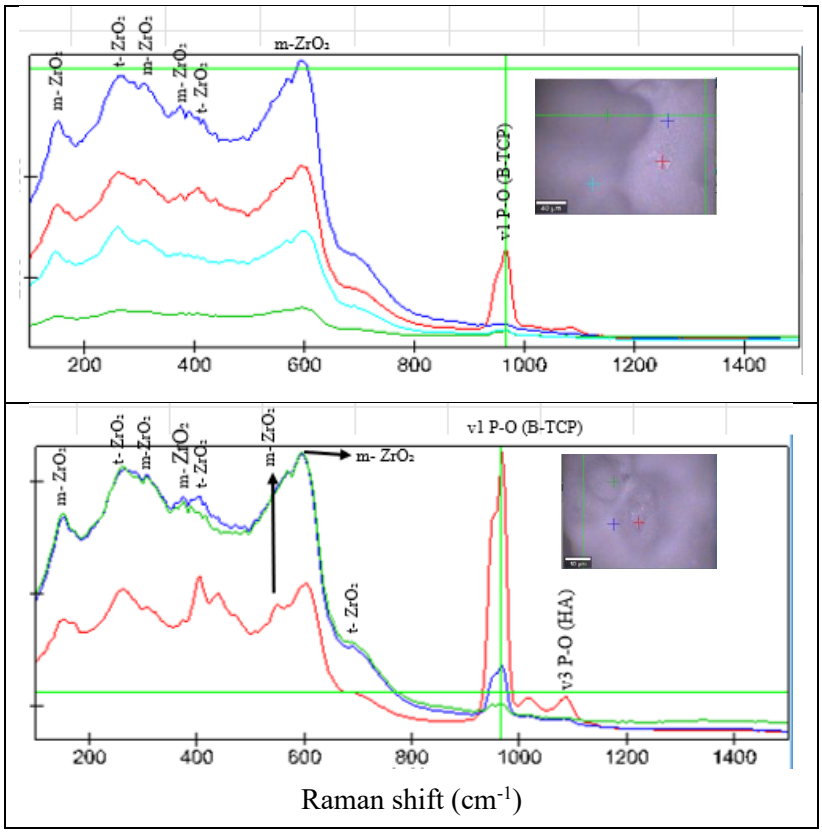

Figure 12- Raman spectra for 25% calcium carbonate type II mixed for 5 minutes with a mixer.

In the case of 35% calcium carbonate type I, represented in Figure 13, m-ZrO_2 peaks are localised at 180 cm^{-1}, 380 cm^{-1} and 600 cm^{-1}, and t-ZrO_2 peaks are 260 cm^{-1} and 650 cm^{-1}. The last peak, 968 cm^{-1}, is v1 P-O (β -TCP).

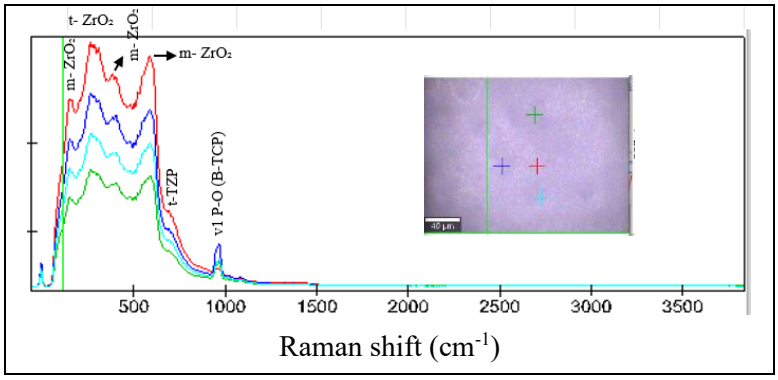

Figure 13- Raman spectrum for 35% calcium carbonate type I for 5 minutes with a mixer.

Figure 14 illustrates the spectrum for 25% calcium carbonate type I mixed with a mixer for 5 minutes. It is possible to see that the peaks associated with yttria-stabilised zirconia are 180 cm^{-1}, 345 cm^{-1}, 380 cm^{-1} and 600 cm^{-1} for m-ZrO_2, 260 cm^{-1} and 650 cm^{-1} for t-ZrO_2. It is also possible to observe a peak at 968 cm^{-1}, v1 P-O (β -TCP).

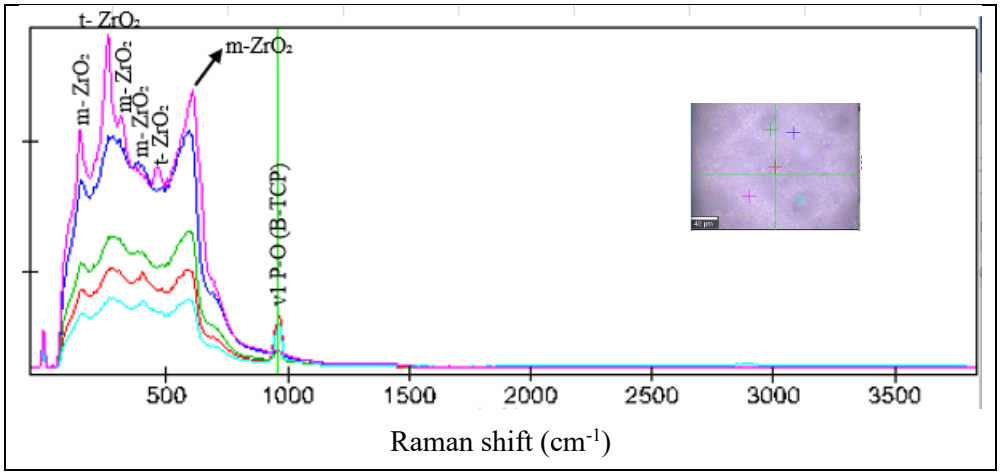

Figure 14- Raman spectrum for 25% calcium carbonate type I mixed for 5 minutes with a mixer.

The following figure, Figure 15, represents the Raman spectra for 20% graphite and 30% calcium carbonate mixed by hand for 5 minutes. The m-ZrO_2 component peaks are at 180 cm^{-1}, 325 cm^{-1} and 600 cm^{-1}, t-ZrO_2 peaks are at 260 cm^{-1}, 410 cm^{-1} and 650 cm^{-1}. The peak at 450 cm^{-1} represents v2 O-Si-O, while the ones at 968 cm^{-1} and 1090 cm^{-1} represent v3 P-O (β -TCP) and v3 P-O (HA), respectively.

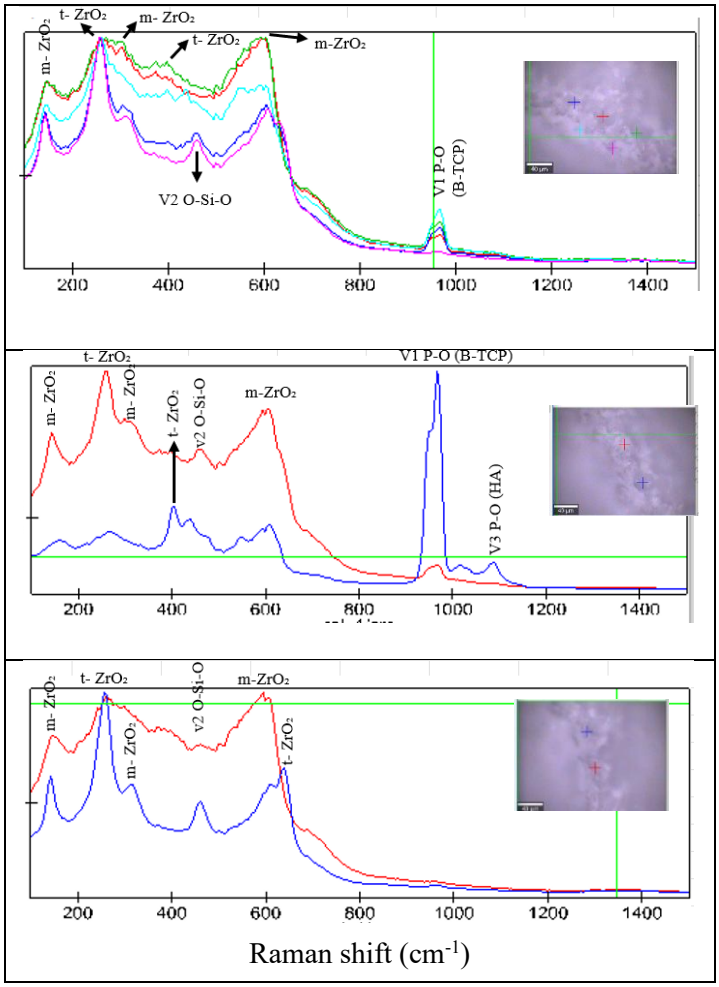

Figure 15- Raman spectrum for 20% graphite and 30% calcium carbonate mixed for 5 minutes with a mixer, in different spots.

Through the Raman analysis, it was possible to confirm that the samples with calcium phosphate contained Zirconia dioxide and the samples with calcium carbonate contained yttria stabilised zirconia, as expected. It is also possible to conclude that independently of the pastes mixture, by hand, with mixer for 5 minutes or 15 minutes, and for the different positions inside the samples, revealing a homogeneous structure, the results show a good uniformity of the composition for all measurements taken.

4

CONCLUSIONS AND FUTURE PERSPECTIVES

4.1 Conclusions

This work aimed to investigate materials that tailored the specific requirements of maxillofacial implants. For this purpose, some parameters were studied, such as the influence of the mixing procedure, the influence of the paste composition on density and mechanical properties.

Besides that, some printing parameters were also evaluated, such as the influence of the needly size and direction of printing.

The mechanical behaviour was evaluated through compression tests, from which Young's modulus and the critical pressure values were determined. The samples with the average Young modulus closest to the literature of trabecular bone are 35% calcium phosphate and 35% calcium carbonate, both of which were autoclaved, and 20% graphite and 30% calcium carbonate type 1. For the cortical bone, the most promising samples was 20% graphite and 30% calcium carbonate.

The samples that presented the lowest Young's modulus and compressive strength values were the samples of full cylinder, both 100% and 50% infill for calcium phosphate and calcium carbonate. The much lower resistance observed may be due to the lower connection between printing lines. As it was not possible to find an article that could corroborate that this happened because of the shape, further tests should be made to understand the reason.

Due to the 90-degree angle of samples for tensile tests that acted as stress concentration points, a premature failure at those locations was observed. For future studies, it is recommended that these sharp corners be replaced with smoother, curved transitions to minimise stress accumulation and improve mechanical performance. The samples must also be larger.

Samples content and prevalent phases, such as Zirconia dioxide, yttria-stabilised zirconia, hydroxyapatite, and β-tricalcium phosphate and in which phase are these constituents. Depending on the composition and way the powder was mixed, it was also possible to evaluate the homogeneity of the samples.

4.2 Future Perspectives

While the current work has provided valuable insights into design and 3D printing of bone-like materials, there remain various aspects that warrant further exploration. This section outlines potential avenues for extending the present research, addressing its limitations, and exploring new questions that have emerged throughout the investigation.

The printing and drying process should be optimised to reduce deformations on the samples. The mixing process using a mechanical mixer should also be optimised, as some samples could not be mixed this way due to poor component integration during stirring.

As mentioned, for the tensile tests, it is recommended to smooth the sharper corners, curved transitions will minimise stress accumulation and improve mechanical performance. Flexural tests should also be conducted to deepen and improve the current understanding of the materials' mechanical behaviour.

For the mechanical analysis to be more accurate, it is recommended that future tests use compression platforms with diameters matching those of the samples.

Further investigation is recommended for certain samples, particularly to the one with 20% graphite and 30% calcium carbonate, as it presented the average Young's modulus value most closely aligned with that of trabecular bone.

Moreover, this study shows potential to eventually be extended to other parts of the body.

BIBLIOGRAPHY

[1] FDA U.S Food and Drug Administration, "Implants and Prosthetics." Accessed: Jan. 03, 2025. [Online]. Available: https://www.fda.gov/medical-devices/products-and-medical-procedures/implants-and-prosthetics

[2] IMPT and Institute of Maxillofacial Prosthetists & Technologists, "What is a prosthesis?" Accessed: Jan. 03, 2025. [Online]. Available: https://www.impt.co.uk/what-is-a-prosthesis/

[3] World Health Organization, "Oral Health." Accessed: Jan. 03, 2025. [Online]. Available: https://www.who.int/news-room/fact-sheets/detail/oral-health

[4] Â. M. L. Pereira, "Ângela Maria Lopes Pereira Reabilitação Oral em Pacientes Maxilectomizados," 2014.

[5] A. T. A. Costa *et al.*, "Reconstrução de Defeitos Ósseos na Região Maxilofacial," *Brazilian Journal of Implantology and Health Sciences*, vol. 5, no. 4, pp. 784–793, Aug. 2023, doi: 10.36557/2674-8169.2023v5n4p784-793.

[6] Marco Bianchini, "O osso alveolar." Accessed: Nov. 22, 2024. [Online]. Available: https://vmcom.com.br/vmblog/o-osso-alveolar/

[7] A. Y. Alqutaibi, M. A. Alghauli, M. H. A. Aljohani, and M. S. Zafar, "Advanced additive manufacturing in implant dentistry: 3D printing technologies, printable materials, current applications and future requirements," Oct. 01, 2024, *Elsevier B.V.* doi: 10.1016/j.bprint.2024.e00356.

[8] B. Sun, Q. Ma, X. Wang, J. Liu, and M. R. M. Rejab, "Additive manufacturing in medical applications: A brief review," *IOP Conf Ser Mater Sci Eng*, vol. 1078, no. 1, p. 012007, Feb. 2021, doi: 10.1088/1757-899x/1078/1/012007.

[9] C. Li, D. Pisignano, Y. Zhao, and J. Xue, "Advances in Medical Applications of Additive Manufacturing," *Engineering*, vol. 6, no. 11, pp. 1222–1231, Nov. 2020, doi: 10.1016/j.eng.2020.02.018.

[10] H. K. Celik, S. Koc, A. Kustarci, N. Caglayan, and A. E. W. Rennie, "The state of additive manufacturing in dental research – A systematic scoping review of 2012–2022," *Heliyon*, vol. 9, no. 6, Jun. 2023, doi: 10.1016/j.heliyon.2023.e17462.

[11] A. A. Raheem *et al.*, "A review on development of bio-inspired implants using 3d printing," Dec. 01, 2021, *MDPI*. doi: 10.3390/biomimetics6040065.

[12] "Dental material research in prosthodontics-Towards developing better and efficient biomimetic materials," 2023, doi: 10.2186/jpr.

[13] B. Rajendran, "DENTAL IMPLANT BIOMATERIALS," *Int J Curr Adv Res*, 2019, doi: 10.24327/ijcar.2019.

[14] M. Panchal, S. Khare, P. Khamkar, and K. Suresh Bhole, "Dental implants: A review of types, design analysis, materials, additive manufacturing methods, and future scope," *Mater Today Proc*, vol. 68, pp. 1860–1867, Jan. 2022, doi: 10.1016/J.MATPR.2022.08.049.

[15] R. Galante, C. G. Figueiredo-Pina, and A. P. Serro, “Additive manufacturing of ceramics for dental applications: A review,” *Dental Materials*, vol. 35, no. 6, pp. 825–846, Jun. 2019, doi: 10.1016/J.DENTAL.2019.02.026.

[16] G. Dias Zarur, “ANÁLISE DE ENSAIOS DE TRAÇÃO DE DIVER-SOS CORPOS DE PROVA METÁLICOS EM DI-VERSOS ESTADO TENSILE TEST ANALYSIS IN DIFFE-RENT METALS TEST SPECIMENS IN SEVERAL STATES.”

[17] I. D. Marinescu and M. Pruteanu, “Deformation and Fracture of Ceramic Materials,” *Handbook of Ceramics Grinding and Polishing*, pp. 50–66, Jan. 2015, doi: 10.1016/B978-1-4557-7858-4.00002-9.

[18] L. G. Zhang, J. P. Fisher, and K. W. Leong, “3D Bioprinting and Nanotechnology in Tissue Engineering and Regenerative Medicine,” in *3D Bioprinting and Nanotechnology in Tissue Engineering and Regenerative Medicine, 2nd ed. Academic Press*, 2015, pp. 1–373.

[19] N. A. Drage, R. M. Palmer, G. Blake, R. Wilson, F. Crane, and I. Fogelman, “A comparison of bone mineral density in the spine, hip and jaws of edentulous subjects,” *Clin Oral Implants Res*, vol. 18, no. 4, pp. 496–500, Aug. 2007, doi: 10.1111/j.1600-0501.2007.01379.x.

[20] F. Bakan, “A systematic study of the effect of pH on the initialization of Ca-deficient hydroxyapatite to β- TCP nanoparticles,” *Materials*, vol. 12, no. 3, Jan. 2019, doi: 10.3390/ma12030354.

[21] S. Komarek, A. Wojteczko, Z. Pędzich, K. Haberko, P. Kwaśniewski, and M. Ziąbka, “Strength stability over loading time of zirconia-hydroxyapatite composites,” *Mater Today Commun*, vol. 37, Dec. 2023, doi: 10.1016/j.mtcomm.2023.106963.

[22] A. Vasilevskaya, O. V. Almjasheva, and V. V. Gusarov, “Peculiarities of structural transformations in zirconia nanocrystals,” *Journal of Nanoparticle Research*, vol. 18, no. 7, Jun. 2016, doi: 10.1007/s11051-016-3494-y.

[23] C. M. Ramos, A. S. Tabata, P. F. Cesar, J. H. Rubo, P. A. S. Fracisconi, and A. F. S. Borges, “Application of micro-raman spectroscopy to the study of yttria-stabilized tetragonal zirconia polycrystal (Y-TZP) phase transformation,” *Appl Spectrosc*, vol. 69, no. 7, pp. 810–814, Jul. 2015, doi: 10.1366/14-07793.

[24] J. A. Muñoz Tabares and M. J. Anglada, “Quantitative analysis of monoclinic phase in 3Y-TZP by raman spectroscopy,” *Journal of the American Ceramic Society*, vol. 93, no. 6, pp. 1790–1795, Jun. 2010, doi: 10.1111/j.1551-2916.2010.03635.x.

[25] S. Tsuchida and T. Nakayama, “Recent Clinical Treatment and Basic Research on the Alveolar Bone,” Mar. 01, 2023, *MDPI*. doi: 10.3390/biomedicines11030843.

[26] “Jaw Bone Loss,” Pacific Oral Surgery. Accessed: Nov. 27, 2024. [Online]. Available: https://www.pacificoralsurgeon.com/jaw-bone-health/jaw-bone-loss/

A

Another Appendix